Available online at www.sciencedirect.com
ScienceDirect
Acta Materialia 59 (2011) 2057–2068
Acta MATERIALIA
www.elsevier.com/locate/actamat

Shear transformation zone volume determining ductile–brittle transition of bulk metallic glasses

F. Jiang [a], M.Q. Jiang [b], H.F. Wang [a], Y.L. Zhao [a], L. He [a], J. Sun [a,*]

[a] State Key Laboratory for Mechanical Behavior of Materials, Xi'an Jiaotong University, Xi'an 710049, China
[b] State Key Laboratory of Nonlinear Mechanics, Institute of Mechanics, Chinese Academy of Sciences, Beijing 100190, China

Received 1 August 2010; received in revised form 17 November 2010; accepted 1 December 2010
Available online 28 December 2010

Abstract

Three-point bending experiments were performed on as-cast and annealed samples of $Zr_{52.5}Cu_{17.9}Ni_{14.6}Al_{10}Ti_5$ (Vit105) bulk metallic glasses over a wide range of temperatures varying from room temperature (293 K) to liquid nitrogen temperature (77 K). The results demonstrated that the free volume decrease due to annealing and/or cryogenic temperature can reduce the propensity for the formation of multiple shear bands and hence deteriorate plastic deformation ability. We clearly observed a sharp ductile-to-brittle transition (DBT), across which microscopic fracture feature transfers from micro-scale vein patterns to nano-scale periodic corrugations. Macroscopically, the corresponding fracture mode changes from ductile shear fracture to brittle tensile fracture. The shear transformation zone volume, taking into account free volume, temperature and strain rate, is proposed to quantitatively characterize the DBT behavior in fracture of metallic glasses.

Keywords: Bulk metallic glass; Shear transformation zone; Tension transformation zone; Free volume; Ductile-to-brittle transition

1. Introduction

Bulk metallic glasses (BMGs) represent a relatively young class of materials envisaged for many functional and structural applications [1–5]. Crystalline alloys usually have the ductile-to-brittle transition (DBT) temperature that is determined by the dislocation movements. Owing to the lack of long-range order, BMGs are free of dislocations and other crystalline defects. It is therefore expected that these materials should not undergo DBT process. However, the DBT phenomena, as first reported by Wu and Spaepen [6], have been widely observed in metallic glasses [7–16]. Due to the practical and scientific significance of this behavior, it has attracted much attention. Possible factors such as free volume [6], strain rate sensitivity [8], Poisson's ratio [14,15] and structural relaxation [11,13] have been thought to be responsible for it. For example, Lewandowski et al. [14,15] correlated the fracture energy of a number of different glasses with Poisson's ratio ν and reported a sharp DBT at the critical $\nu = 0.31$–0.32. Kumar et al. [13] argued that the embrittlement of BMGs subjected to annealing below and above the glass transition temperature was due to structural relaxation and crystallization, respectively. Very recently, the Ramamurty group [16] performed a series of impact toughness tests on as-cast and structurally relaxed Zr-based BMGs at various temperatures. They demonstrated a sharp DBT temperature that was sensitive to the free-volume concentration in BMGs. In particular, they speculated that such DBT could be understood as the change in the nature of the transformation zones from shear transformation zones (STZs) to tension transformation zones (TTZs), which was proposed by one of the authors as given in Ref. [17]. Their findings provide a general physical picture of the DBT behavior in metallic glasses. However, the more quantitative analyses about this aspect and the underlying precise nature deserve to be studied.

* Corresponding author. Tel.: +86 02982667143; fax: +86 02982663453.
E-mail address: junsun@mail.xjtu.edu.cn (J. Sun).

1359-6454/$36.00 © 2010 Acta Materialia Inc. Published by Elsevier Ltd. All rights reserved.
doi:10.1016/j.actamat.2010.12.006

In this work, we chose a Zr-based BMG as a model material, focusing on the inhomogeneous flow and the DBT behaviors in the fracture of BMGs. Three-point bending tests were conducted on the as-cast and annealed samples at temperatures ranging from 293 K down to 77 K. We found that either the structural annealing or the temperature decreasing could reduce the number density of shear bands and the resultant plastic deformation. A significant DBT behavior in fracture from STZ-mediated micro-scale vein pattern to TTZ-dominated nano-scale periodic corrugation was observed in the annealed samples bent at the cryogenic temperature. We argue that the STZ volume is a key to determining the DBT behavior in the fracture of BMGs based on the cooperative shearing model (CSM) proposed by Johnson and Sawmer [18] as well as the physical picture of STZ vs. TTZ in fracture of BMGs [16,17].

2. Experimental methods

The master ingots of $Zr_{52.5}Cu_{17.9}Ni_{14.6}Al_{10}Ti_5$ (Vit105) were produced by arc-melting Zr of 99.8% purity and Cu, Ni, Al and Ti of 99.99% purity in a Ti-gettered argon atmosphere. Plates with dimensions of $50 \times 20 \times 1.5$ mm were prepared using the drop casting method. In order to reduce the free volume content, some as-cast samples were sealed in an evacuated quartz capsule and annealed for 15 min at temperatures of 503 K, 553 K, 593 K, 623 K and 653 K below the glass transition temperature T_g (683 K at the heating rate of 0.33 K s^{-1}), respectively. In addition, some as-cast samples were annealed for a longer time of 48 h at 653 K to remove the free volume content as far as possible. The microstructure of these samples was identified through high resolution transmission electron microscope (HRTEM; JEOL Ltd. JEM-2100F). The free volume changes were indirectly measured using the differential scanning calorimetry (DSC) method [19,20]. The DSC tests were conducted using a Setaram DSC 2000 with a 800 °C rod at a heating rate of 0.33 K s^{-1} in a flow of argon, and a second run under identical conditions was used to determine the base line after each measurement. All three-point bending samples have the same dimensions of $20 \times 4 \times 0.8$ mm through symmetric milling from two surface sides to center. The bending test was conducted on a computer-controlled SANS testing machine at a displacement rate of 0.02 mm min^{-1}. The span was 10 mm. During testing, the load–deflection (P–δ) curves were recorded. Four group bending tests were undertaken to evaluate the plastic deformation ability of these samples:

1. as-cast and 15 min annealed samples were tested at room temperature (293 K);
2. as-cast samples were tested at different cryogenic temperatures (273 K, 252 K, 218 K, 159 K and 77 K);
3. some 15 min annealed samples were tested at 77 K; and
4. 653 K longer-time-annealed samples were tested at room temperature (293 K).

During the cryogenic temperature test, the sample, together with pushrod and supports, was immersed in a cryogenic liquid tank. We adjusted the cooling mixtures with ethanol and liquid nitrogen or dry ice (CO_2) within the tank to achieve the desired temperature between 77 K (liquid nitrogen) and 273 K. The tensile surface under bending was previously polished in order to observe the shear band with scanning electron microscopes (SEM; JEOL Ltd. JSM-6700F and Hitachi S-2700) after test.

3. Results

Fig. 1 shows the HRTEM images and corresponding selected area electron diffraction patterns of as-cast sample and relaxed Vit105 samples. For the as-cast sample, neither nanocrystallization nor nanometer-sized phase separation was detected within the experimental uncertainty of the techniques used, as shown in Fig. 1a, indicating its homogeneous amorphous structure. Fig. 1b shows the HRTEM results of the sample with 653 K annealing for 48 h (the highest annealing temperature plus the longest time among all samples in studied), which confirms that the present annealing regime, which was below the T_g, did not change the amorphous nature of the sample. It is well known that nanocrystallization in the as-cast sample does not readily take place when it is subjected to the electron beam radicalization during the HRTEM experiment. However, for the annealed sample, there is a tendency that nanocrystallization will be more prone to take place with the increase of annealing temperature or annealing time during HRTEM experiment. For instance, when radicalization time lasted for about several seconds, nanocrystallization in the sample with 653 K annealing for 48 h was detected.

Fig. 2 displays the DSC curves of the as-cast samples and the annealed samples. All samples exhibit very similar thermal behavior with a distinct glass transition and a wide supercooled liquid region before crystallization. However, the exothermic signals before glass transition in DSC curves are quite different among these samples, as indicated in the inset to Fig. 2. It is well known that prior to T_g, the exothermic event (i.e. the heat release during relaxation) is indicative of the existence of free volume in BMGs [20]. The as-cast sample shows the largest exothermic enthalpy (ΔH), suggesting the existence of a fairly large amount of free volume Δv_f, where $(\Delta H)_{fv} = \beta' \cdot \Delta v_f$ with a constant β'. For the annealed samples, their exothermic enthalpy values decrease with the increase of the annealing temperature. In particular, the DSC curves of the two 653 K annealed samples (for 15 min and 48 h), in contrast, do not display exothermic signals any more in the same temperature region; this implies that the free volume in the samples were almost annealed out.

Considering the HRTEM and DSC results together, we suggest that the present annealing below T_g has reduced free volume content less or more but has not introduced crystallization yet. Among all the samples, the sample with 653 K annealing for 48 h has the least free volume left and

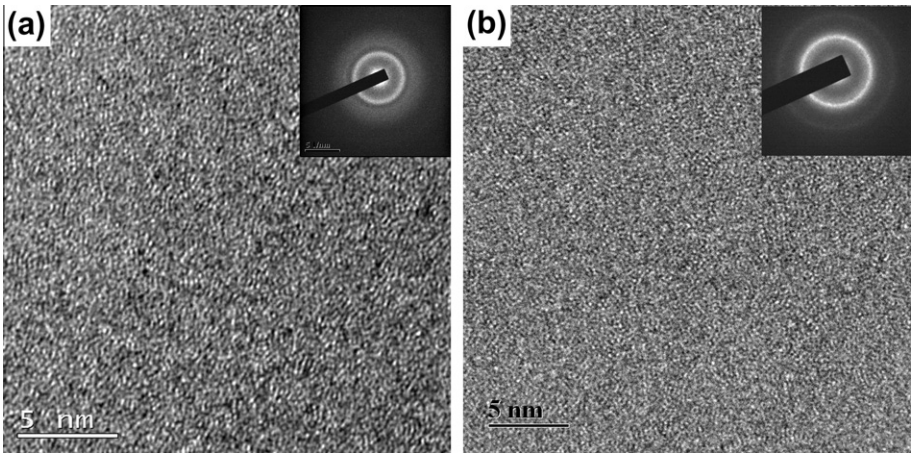

Fig. 1. Bright-field TEM images and corresponding SAED patterns of Vit105 samples (a) as-cast, (b) 653 K annealed for 48 h.

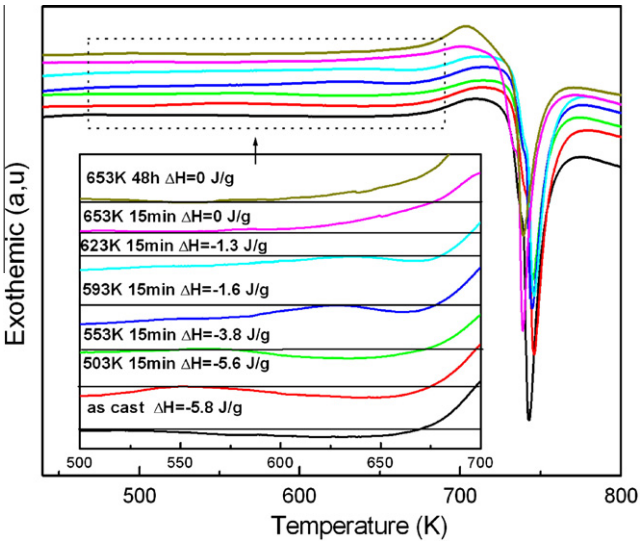

Fig. 2. DSC curves of Vit105 samples at a heating rate of 0.33 K s^{-1}; the inset shows the different exothermic signals before glass transition in DSC curves among these samples.

is very close to its crystalline counterpart for the energy landscape viewpoint [21]. It is noted that the free volume decrease due to annealing really corresponds to the structural relaxation to a lower energy level and more stable state. According to the free volume theory [22], the microstructure change due to relaxation can be described in terms of the free volume.

Fig. 3a displays the flexural stress–deflection curves of as-cast and 15 min annealed samples (Group 1) under three-point bending tests at room temperature. The plastic deflection values were used to reflect their plastic deformation ability [19,23]. The plastic deflection decreased (Fig. 3b) and the flexural yield stress increased with the increase of annealing temperature, i.e. decrease of free volume content. In particular, the 653 K annealed samples with almost free volume annealed out exhibited no plastic deformation before failure. Fig. 3c shows the flexural stress–deflection curves of the as-cast samples tested at room temperature down to liquid nitrogen temperature (77 K) (Group 2). The plastic deflection decreased (Fig. 3d) and the flexural yield stress increased with the decrease of test temperature.

In order to evaluate the different ability to plastic deformation owing to either annealing or cryogenic temperature, we further performed SEM observations for shear band morphology on low tensile side surfaces and fracture pattern on resultant fracture planes. Fig. 4a–f correspond to the as-cast, 503 K annealed and 653 K annealed samples tested at room temperature, respectively. Fig. 5a–d correspond to as-cast sample tested at 159 K and 77 K, respectively. Since the plastic strain of BMGs mainly concentrates on shear bands, the shear band density will also well reflect the plastic deformation ability. Moreover, the tensile fracture surface of the sample usually consists of a smooth region caused by sliding shear and a micron-scaled vein-like pattern region caused by subsequent catastrophic failure [24]. The smooth region corresponds to the critical shear displacement for crack nucleation occurring in shear bands [25–27]. This shear displacement is, to some extent, proportional to the plastic deflection [19,23].

It can be found from Fig. 4 that both the shear band density on the low tensile side surfaces and the critical shear displacement on the fracture surfaces at the tension end decreased with an increase in the annealing temperature, or decreasing free volume. This degrades the macroscopic plastic deformation, which is in agreement with the plastic deflection results (see Fig. 3a and b). For example, the as-cast sample with the highest free volume content shows the densest shear bands (Fig. 4a) and the largest critical shear displacement of ~40.5 μm (Fig. 4b), corresponding to the best plasticity with the plastic deflection of ~0.76 mm (Fig. 3b). Comparing with the as-cast samples, the 503 K annealed sample with less free volume content exhibits reduced number of shear bands (Fig. 4c) and a smaller critical shear displacement of 21.3 μm (Fig. 4d), corresponding to an inferior plastic deformation of ~0.53 mm (Fig. 3b). The 653 K annealed sample with almost no free volume displays only one dominated shear band (Fig. 4e) and the smallest

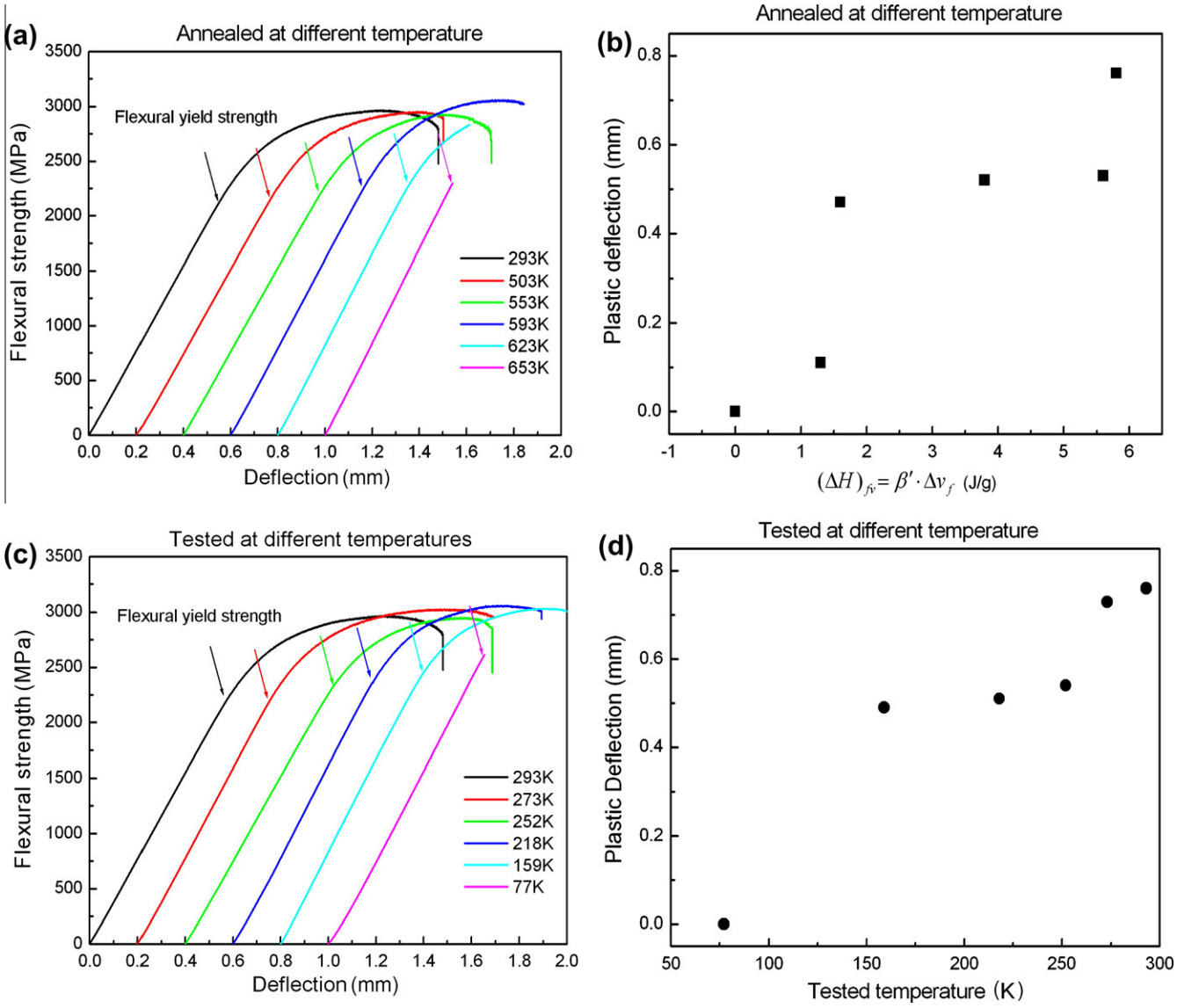

Fig. 3. Flexural stress vs. deflection curves of (a) samples subjected different annealing temperature and (c) as-cast samples tested at different temperatures; variations of plastic deflection with (b) enthalpy release, i.e. free volume and (d) test temperature.

critical shear displacement of 7.3 μm (Fig. 4f); the resultant macroscopic deformation shows only the elastic region without any ductility, as indicated in Fig. 3a. Moreover, it is noted that some striations with average spacing of about several hundred nanometers exist at the beginning portion of the smooth region of the as-cast samples. See the inset to Fig. 4b. However, as for the other relaxed samples, striations can gradually reduce and even disappear on the smooth regions, as shown in the insets to Fig. 4d and f, respectively. It is suggested that the striations are the result of the competition between initiating new shear bands at other sites near the main shear band and reactivating new shear banding events on previously formed shear bands [19,28]. The gradual disappearance of serrations implies that the shear band forms with more difficulty and samples were prone to shear fracture rather than shear slide due to the decrease of free volume content.

Similarly, for the samples in Group 2, with the decrease of the test temperature, both the shear band density on the low tensile side surface and the critical shear displacement on the resultant fracture surface also gradually decreased. Compared with the as-cast sample tested at room temperature (Fig. 4a and b), the 159 K tested sample has fewer shear bands (Fig. 5a) and smaller critical shear displacement of 17.5 μm (Fig. 5b). The 77 K tested sample shows no other shear bands besides the main shear band (Fig. 5c) and has critical shear displacement of 10.8 μm (Fig. 5d). In addition, serrations also gradually reduce and even disappear on the smooth regions in the samples tested at low temperatures (see the insets to Fig. 5b and d).

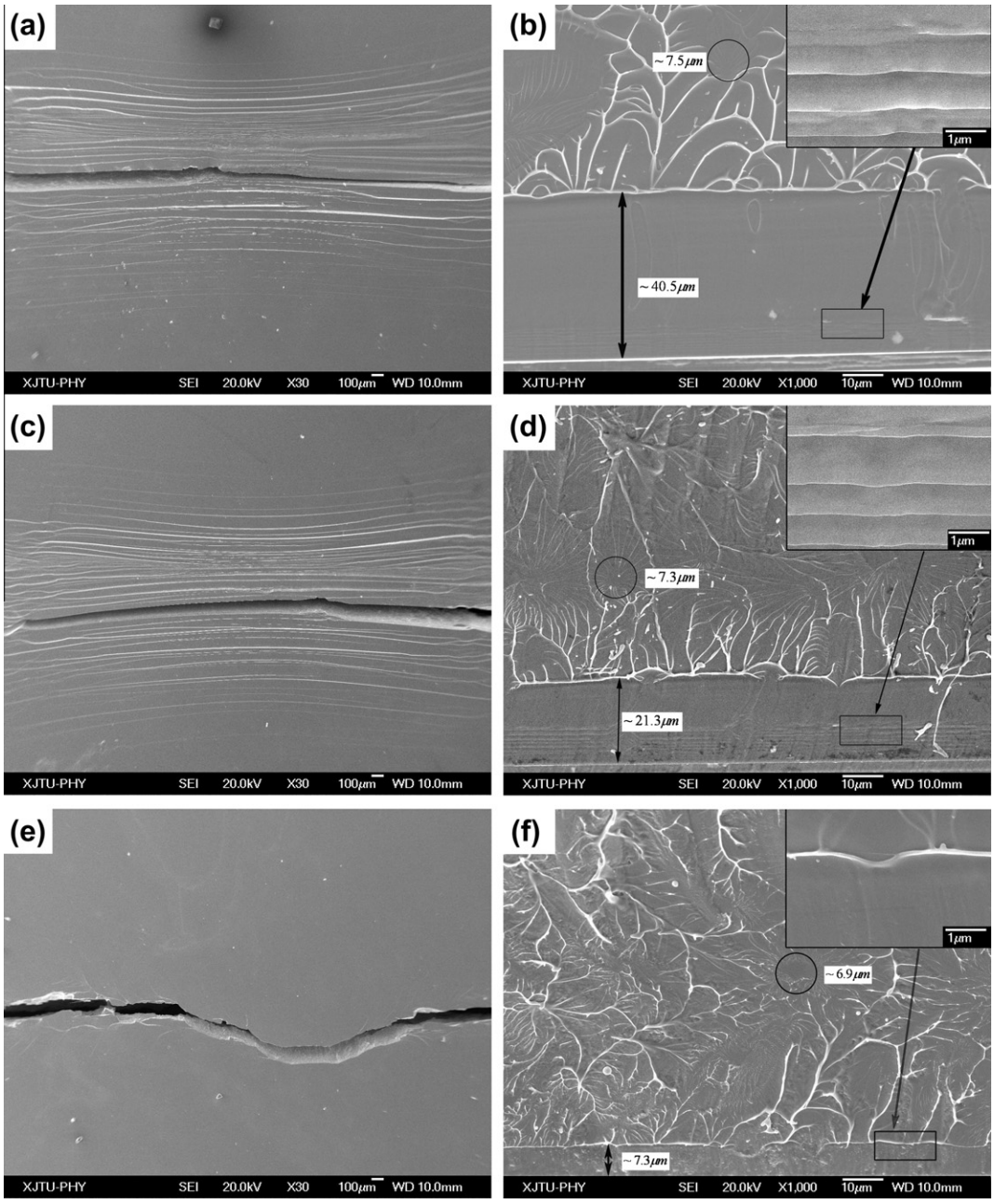

Fig. 4. Appearance of tensile lower surface (left column) and tensile side fracture surfaces (right column) in plates with different thermal treatment states tested at room temperature (Group 1): (a and b) for as-cast samples, (c and d) for 503 K 15 min annealed samples and (e and f) for 653 K 15 min annealed samples.

Furthermore, it is worth noting that the micro-scale vein pattern dominates all fracture surfaces of Groups 1 and 2 regardless of whether there is good plastic deflection or not (as shown in Figs. 4b, d and f and 5b and d). Here, the ridge spacing (w) found on the fracture surface was used to calculate the fracture toughness (K_c) with the Dugdale approximation [29,30]

$$w = \frac{1}{6\pi}\left(\frac{K_c}{\sigma_y}\right)^2 \tag{1}$$

where σ_y is yield strength and can be estimated through Vickers hardness H_V with a relation of $\sigma_y = H_V/3$. H_V of the as-cast and 653 K annealed samples are ~4.77 GPa and 5.15 GPa, respectively. Since both annealing process and low temperature will enhance the yield strength of the samples, all involved other samples will have larger yield strength than that of the as-cast sample. Then we can obtain that the above samples have fracture toughness (K_c) of ~18 MPa $\sqrt{\text{m}}$ at least, where w is ~7 μm and yield strength σ_y is taken ~1590 MPa. It implies that, for

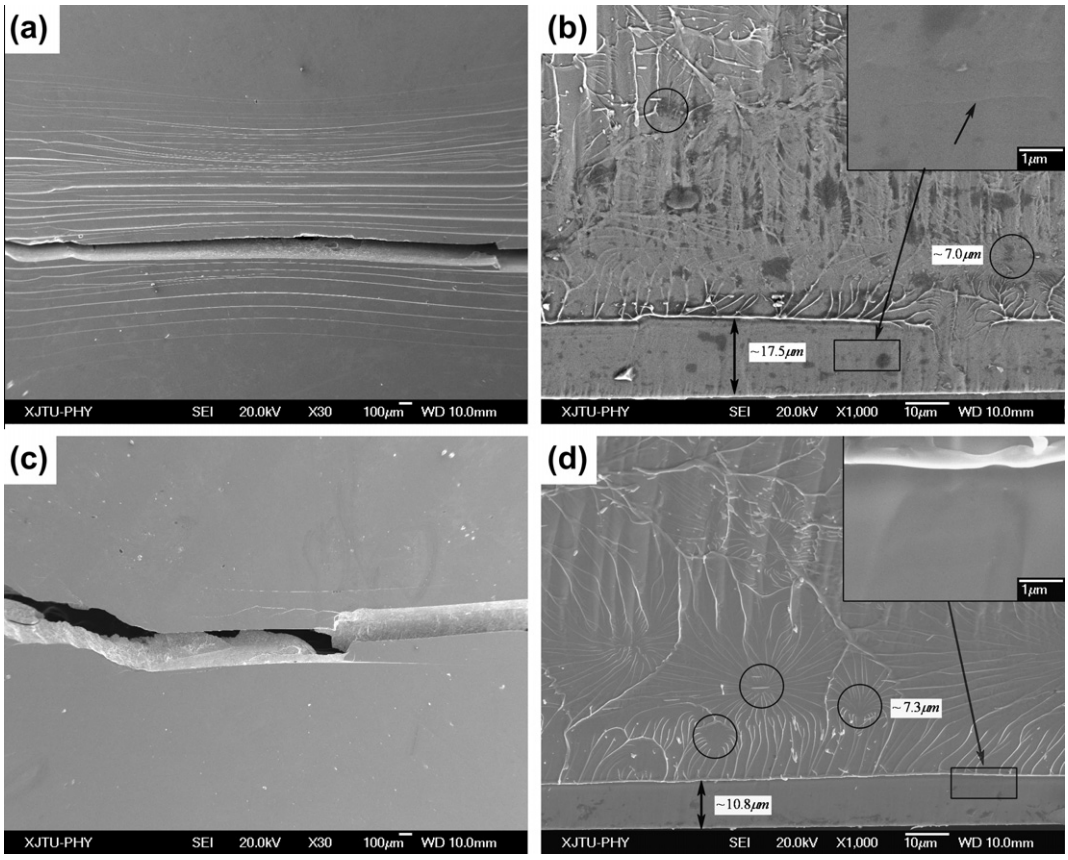

Fig. 5. Appearance of tensile lower surface (left column) and tensile side fracture surfaces (right column) of as-cast samples tested at different temperatures: (a and b) for 159 K, (c and d) for 77 K.

Groups 1 and 2, either annealing process or cryogenic temperature has reduced plasticity (in terms of formation of multiple shear bands) but not thoroughly deteriorated fracture toughness yet.

We further performed the bending tests for Group 3 (the 15 min annealed samples at cryogenic temperature 77 K) to investigate the coupling effect of annealing and cryogenic temperature. All tested samples failed without plastic deflection as shown in Fig. 6. Even the strength at fracture has also decreased. There are few shear bands on the low tensile surfaces of all samples (as shown in Fig. 7a, c and e) and the critical shear displacements (marked in Fig. 7b, d and f) decrease with the increase of annealing temperature, i.e. free volume decrease. In general, the fracture surfaces still consist of micron-scaled smooth region and micro-scale vein pattern region as shown in Fig. 7b and d (for 503 K, 593 K annealed samples tested at 77 K). However, for the 653 K annealed sample tested at 77 K, the smooth region decreases to only ~190 nm and nano-scale periodic corrugations, rather than the micro-scale vein patterns, appeared on the fracture surface as indicated in Fig. 7f. Similar nano-scale periodic corrugations have also been found on the fracture surfaces of high-velocity plate impact tests of Vit1 [17], the brittle Mg-based BMGs [31,32] and the impact test samples of relaxed Zr-based BMG [9,10,16,33]. The fracture toughness K_c of this 653 K annealed sample at 77 K was calculated to be ~1.3 MPa $\sqrt{m}$ through Eq. (1), where ridge spacing $w \approx 50$ nm (see Fig. 7f) and yield strength σ_y is taken to be 1700 MPa (see Fig. 6). Such low fracture toughness is comparable to those of brittle Mg-based

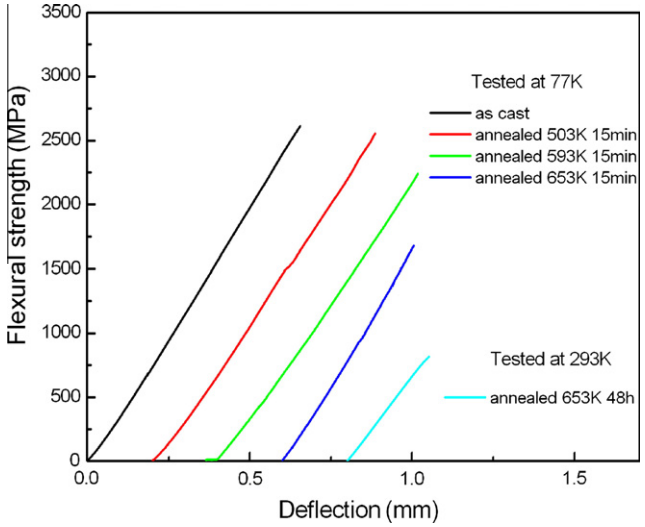

Fig. 6. Flexural stress vs. deflection curves of some 15 min annealed samples tested at 77 K and the sample annealed at 653 K for 48 h tested at room temperature (293 K).

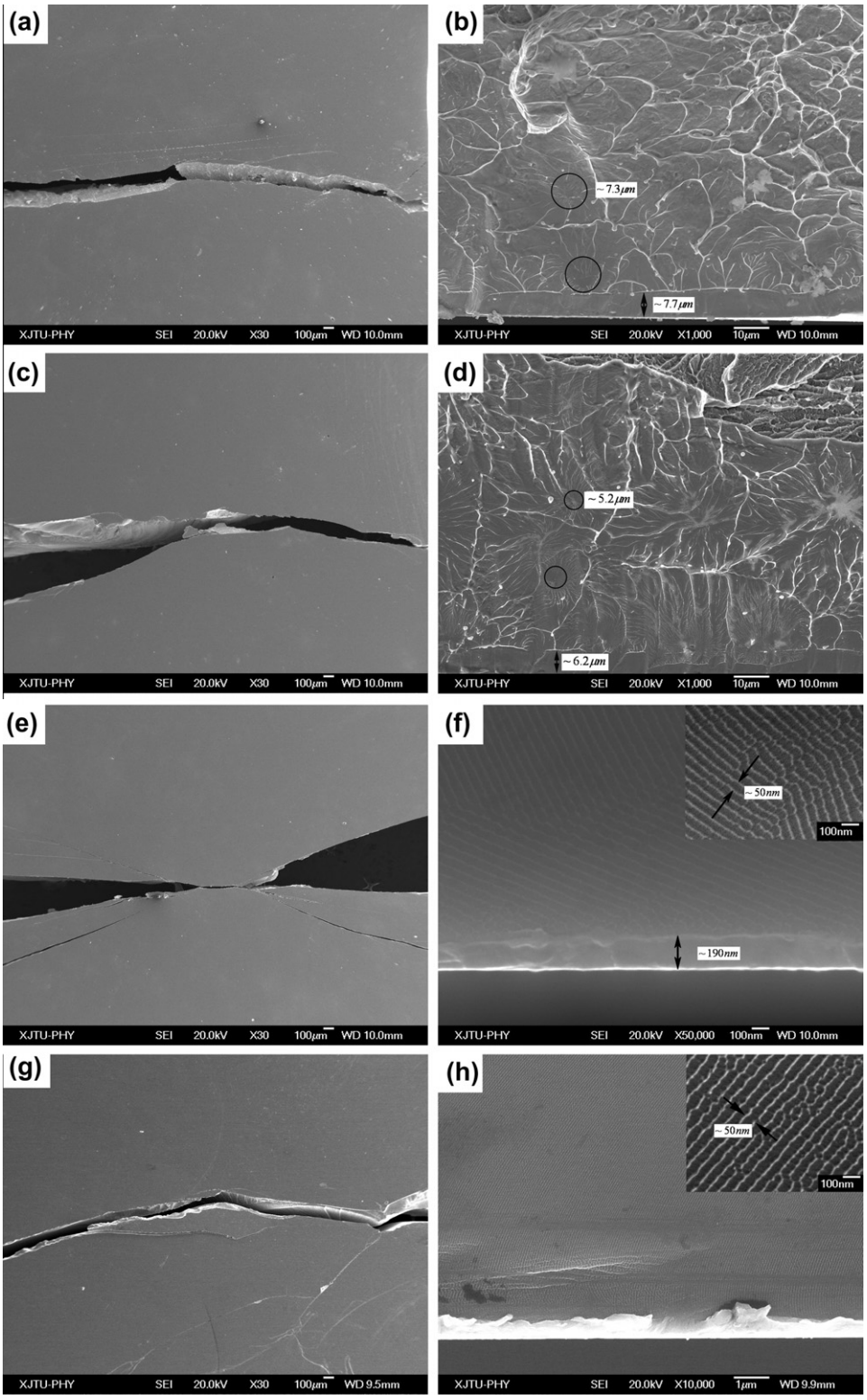

Fig. 7. Appearance of tensile lower surface (left column) and tensile side fracture surfaces (right column): (a and b) for 503 K 15 min annealed sample tested at 77 K, (c and d) for 593 K 15 min annealed sample tested at 77 K, (e and f) for 653 K 15 min annealed sample tested at 77 K, and (g and h) for 653 K, 48 h annealed sample tested at 293 K.

BMGs and silicate glasses (1–2MPa $\sqrt{\text{m}}$). Jiang et al. [17] has proposed that the nano-scale periodic corrugation is a typical feature of "quasi-cleavage" fracture that is a result of rupturing of tension transformation zones (TTZs) with STZs in the background ahead of the crack tip. The TTZ is essentially a local atomic cluster similar in size to an

STZ but with smaller relaxation timescales and less viscoplasticity. It therefore means that the TTZs are more amenable to fracture than flow when subjected to stress [16,17].

Accounting for the results of 653 K 15 min annealed samples at the room temperature and 77 K together, we found that the cryogenic temperature has accelerated the ductile-fracture to brittle-fracture transition (see Figs. 4e and f and 7e and f). Next, we prolonged the annealing time from 15 min to 48 h at 653 K in order to remove the free volume content as far as possible. When the long-time-annealed sample was tested under bending at room temperature (293 K), it failed catastrophically before reaching its yield point with fracture strength only ~1000 MPa, which is more inferior to that of other samples (above 2000 MPa) as shown in Fig. 6. SEM observation demonstrated that there is no shear band instead of a tension crack on the low tensile side surface as shown in Fig. 7g. The resulting facture surface was very smooth and nanoscale periodic corrugations were also found as shown in Fig. 8h, which is similar to that of the 653 K 15 min annealed sample tested at 77 K (see Fig. 7e and f).

Finally, we revisit the macro-fracture modes of these samples, which are presented in Fig. 8. The as-cast sample tested at room temperature (Fig. 8a) and the 653 K 15 min annealed sample tested at room temperature (Fig. 8b) both showed the ductile shear fracture mode with a typical tensile fracture angle of ~51–53° [34]. However, for the 653 K 15 min annealed sample tested at 77 K (Fig. 8c) and the 653 K 48 h annealed sample (with free volume completely annealed out) tested at room temperature (Fig. 8d), they both failed in a brittle tensile fracture mode with fracture angles ~90°, clearly indicating a cleavage cracking [35]. Thus we can conclude that either the structural annealing or the temperature decrease can reduce the propensity for the formation of multiple shear bands and hence degrade plastic deformation ability, and even induce a significant DBT in BMGs. It is should be noted that in the present work, we defined the DTB as follows: microscopic fracture feature transfers from micro-scale vein patterns to nanoscale periodic corrugations. Macroscopically, the corresponding fracture mode changes from shear fracture to brittle tensile fracture. This definition is more intrinsic than that based on the macroscopic plastic strain. Therefore, some samples show no permanent plastic strain under bending test (as shown in Figs. 3a and c and 6); however, the micro-scale vein patterns are dominant on the fracture surfaces of these samples (as shown in Figs. 4b, d and f, 5b and d and 7b and d). This implies that although they suffer a macroscopically brittle failure, there is clear evidence that they are capable of legitimate plastic shear flow at the micro-scale. Such macro–micro inconsistency results from the strong tendency for shear flow localization in these samples during tests. The shear localization in BMGs usually occurs at ~10 nm scale [36], which cannot lead to appreciable plastic flow at macroscopic scale. Based on the definition of DTB presented above, we suggest that

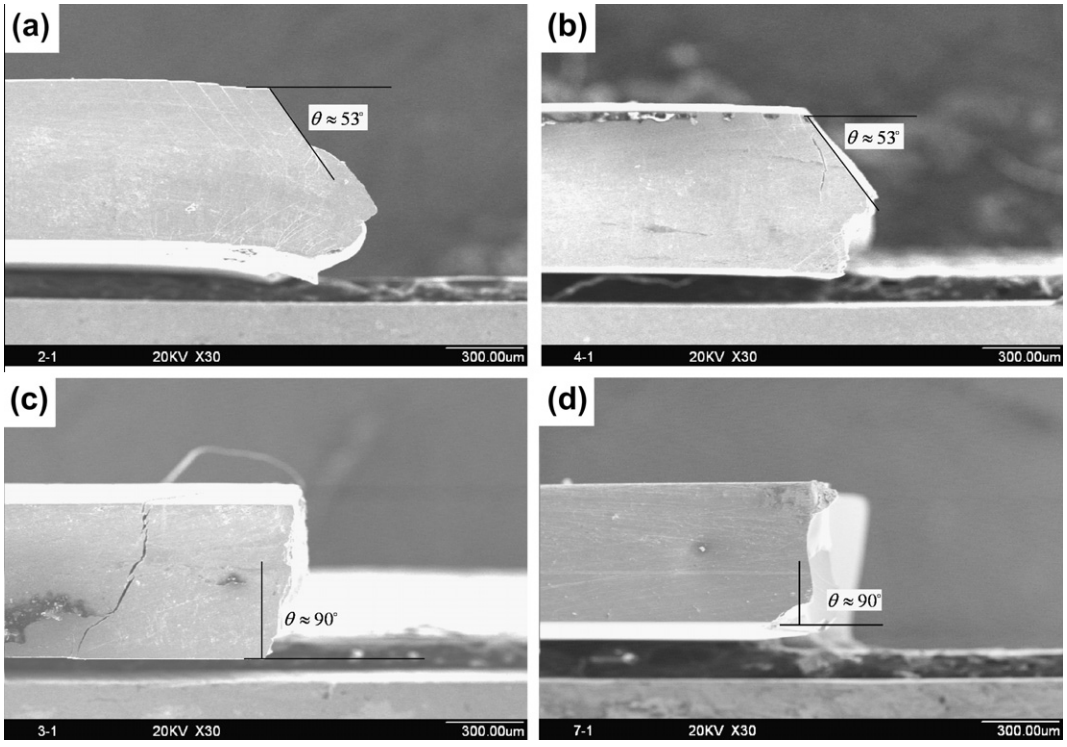

Fig. 8. The macro-fracture modes of (a) as-cast sample tested at room temperature, (b) 653 K 15 min annealed sample tested at room temperature, (c) 653 K 15 min annealed sample tested at 77 K and (d) 653 K 48 h annealed sample with free volume completely removed out tested at 293 K. (a and b) Failed in a shear fracture mode in ductile and (c and d) failed in a tensile fracture mode in brittle.

these samples still failed in a ductile shear mode rather than a brittle tensile mode, even though they show no macroscopic plastic strain in their bending curves.

4. Discussion

In this section, we shall identify the underlying mechanism of such DBT behavior described previously. It has been recognized that macroscopic flow of metallic glasses occurs as a result of a series of STZ operations. In other words, yielding occurs when the applied activation energy causes a critical density of STZs to become unstable [18]. According to cooperative shear model (CSM) proposed by Johnson et al. [18,37], only when the barrier crossing rate of STZs reaches a critical value comparable to applied strain rate, $\dot{\gamma}$, does the plastic deformation takes place. This yields

$$C\dot{\gamma} = \omega_0 \exp\left(-\frac{W_\tau}{kT}\right) \tag{2}$$

where W_τ is the barrier energy for an STZ at finite stress, ω_0 is an attempt frequency, C is a dimensionless constant of order unity, k is the Boltzmann constant and T is the temperature.

In general, STZ is aided by the free volume available in the material and initiates at the site where free volume abounds. An activation factor $\exp\left(-\frac{\Delta V^*}{V_f}\right)$, which is statistically related to free-volume concentration [4,22,38], could be added into Eq. (2). We then have

$$C\dot{\gamma} = \omega_0 \exp\left(-\frac{W_\tau}{kT}\right)\exp\left(-\frac{\Delta V^*}{V_f}\right) \tag{3}$$

where ΔV^* is required excess free volume to transition and should be at least larger than atom volume, and V_f is the average free volume per particle and is dependent on the historic state. For example, higher cooling rate will induce a larger V_f, whereas annealing process will decrease it.

It is noted that Eq. (3) has similar form to the general flow equation proposed by Spaepen [22] within the free volume formulism. In our present analysis, the hyperbolic sine form $\sinh\left(\frac{\tau V}{kT}\right)$ was omitted because the initiation of an operating shear band is a non-steady-state event that is generally not accompanied by a back-flux of shear events. W_τ is the barrier energy for an STZ operation rather than an individual atom motion. At the same time, the term $\exp\left(-\frac{\Delta V^*}{V_f}\right)$ is the configurational probability for an STZ zone, not just for a single atom [38]. A similar equation relating STZ with free volume has also been put forward by Schuh et al. [4] and Jiang et al. [39]. Following Johnson and Samwer [18], the activation energy for an STZ is given by

$$W_\tau = 4R\mu_T\gamma_T^2(1-\tau/\tau_C)^{3/2}\zeta\Omega \tag{4}$$

In this equation, μ_T is the temperature-dependent shear modulus, expressed by $\mu_T = \mu_0 - d\mu_0 T/\mathrm{d}T \times T\,(\mathrm{GPa/K})$ with the athermal shear modulus μ_0. The yield elastic limit has the form $\gamma_T = 0.036 - 0.016\,(T/T_g)^{2/3}$. $\tau = 2\mu_T\gamma_T/\pi$ is the applied shear stress at yielding where the nonlinear elastic response of an STZ is considered as τ increases from 0 to τ_C, where $\tau_C = \mu_0\gamma_0 = 0.036\ \mu_0$ is the threshold shear resistance at 0 K. Constant R is the "fold ratio" $\approx 1/4$ and $\zeta = 3$ is a correction factor. Ω is the actual STZ volume. Using Eqs. (3) and (4), the STZ volume can now be determined

$$\Omega = \frac{k}{4R\zeta\mu_T\gamma_T^2(1-2\mu_T\gamma_T/(\pi\mu_0\gamma_0))^{3/2}}T\left(\ln\frac{\omega_0}{C\dot{\gamma}} - \frac{\Delta V^*}{V_f}\right) \tag{5}$$

For a specific BMG, we can find that Ω is mainly dependent on three factors: (i) $\ln\frac{\omega_0}{C\dot{\gamma}}$, which measures the competition between external applied loading rate and internal activation rate of STZs, (ii) the ambient temperature T, and (iii) the free volume $\frac{\Delta V^*}{V_f}$ within materials. It is important to point out that we set the shear strain rate to be equal to the applied strain rate $\dot{\gamma}$ in determining the STZ size (Eq. (5)), which is derived from the CSM (Eq. (2)) [18]. It is worth noting that the CSM deals only with the onset of (inhomogeneous) plastic yielding rather than the post-yielding behavior, namely, the shear-banding process, when BMGs are subjected to macroscopic strain rate $\dot{\gamma}$. In fact, recent works [40–42] have demonstrated that the local shear strain rates within the band can significantly exceed the applied strain rate.

As pointed by Pan et al. [43], a large STZ volume Ω, when compared with a small one, enables a fewer number of STZs to be activated for the nucleation of a shear band. Moreover, the large-size flow units in plastic deformation can produce large internal concentrations of the applied stress where thermally activated production of new flow becomes easy [44]. When the STZ volume Ω is extremely small or close to zero, it will need a large number of STZs and it might be hard to synchronously cooperate shearing to generate a shear band, whereas brittle TTZ mode will occur instead of the STZ mode. Therefore, the STZ volume Ω could be a key factor to generate shear bands and thus the shear deformation. In the following, we shall discuss the effects of the three factors just mentioned above on the STZ volume in detail.

Jiang et al. [17] have performed the high-velocity plate impact tests of as-cast Vit1 BMG at room temperature and found the transition of STZ mode to TTZ mode at a higher strain rate of $10^6\ \mathrm{s}^{-1}$. Once TTZ operations occur, we can consider that $\Omega \to 0$. According to Eq. (5), this results in a critical condition for DBT

$$\ln\frac{\omega_0}{C\dot{\gamma}} - \frac{\Delta V^*}{V_f} \to 0 \tag{6}$$

In the quasi-static strain rate range (10^{-4}–$10^{-2}\ \mathrm{s}^{-1}$), $\ln\frac{\omega_0}{C\dot{\gamma}} \approx 30$ [18]. As the dynamic strain rate of $10^6\ \mathrm{s}^{-1}$, it is $\sim 10^8$–10^{10} times higher than the strain rate of 10^{-4}–$10^{-2}\ \mathrm{s}^{-1}$. In such a case, $\ln\frac{\omega_0}{C\dot{\gamma}} \approx 10$. Therefore, we can obtain $\frac{\Delta V^*}{V_f} \approx 10$ for the as-cast Vit1. This predicted value is very

close to that $\frac{\Delta V^*}{V_f} \approx 14$ in the numerical simulation of Falk and Langer [38]. As for the present Vit105 BMGs, we roughly consider that its as-cast state has free volume the same as the as-cast Vit1, that is, $\ln\frac{\omega_0}{C\dot{\gamma}} - \frac{\Delta V^*}{V_f} = 20$. If we choose the shear modulus at room temperature for Vit 105 $\mu_0(T_R) = 31.8$ GPa, and $d\mu_{0T}/dT$ 4×10^{-3} (GPa/K), we can obtain $\mu_0 = 33$ GPa. Thus, we have the STZ volume Ω for the as-cast Vit105 that depends only on the temperature T

$$\Omega = \frac{6.667kT}{(33 - 0.004T)(0.036 - 2.063 \times 10^{-4}T^{2/3})^2(1 - 0.5359 \times (33 - 0.004T)(0.036 - 2.063 \times 10^{-4}T^{2/3}))^{3/2}} \quad (7)$$

According to Eq. (7), we calculated $\Omega \approx 2.94$ nm^3 for the as-cast Vit105 at room temperature (293 K). This value is very close to the experimental results of Pan et al. [43]. Moreover, it indicates that an STZ for as-cast sample at room temperature contains ~158 atoms, when using an average Goldschmidt radius of 0.16 nm [45]. The value is well consistent with other experimental measurements and simulations [4,18,38–39,43–48], where typical values between a few and roughly 100 atoms have been reported.

Current experimental results show that when the sample was subjected to annealing to remove free volume as far as possible, the macro-fracture mode at room temperature has changed from shear fracture mode to tensile fracture mode (see Fig. 8d). At the same time, micro-fracture feature has also changed from STZ-mediated vein patterns to TTZ-dominated nano-scale periodic corrugations (see Fig. 7h). Such DBT also requires the critical condition, that is, $\Omega \to 0$. Due to $\ln\frac{\omega_0}{C\dot{\gamma}} \approx 30$ for the quasi-static strain rates, the critical condition leads to $\frac{\Delta V^*}{V_f} \approx 30$ that free volume is almost completely annealed out. It is reasonable to speculate that $10 \leqslant \frac{\Delta V^*}{V_f} \leqslant 30$ should correspond to different free volume state between the as-cast sample and the 653 K 48 h annealed sample that can be as a reference sample.

For the as-cast sample tested at 77 K, we obtain that the STZ volume Ω is ~0.73 nm^3 based on Eq. (7), which contains ~39 atoms. Now we revisit the fracture features of the as-cast sample at 77 K and the 503 K annealed sample at 77 K. See Figs. 5d and 7b. We find that the shear offset values of the former are only a little larger than that of the latter, which is agreement with their difference between their free volume ($(\Delta H)_{fv} = \beta' \cdot \Delta v_f$). We assume that they have the same difference of STZ volume as that of the free volume. Considering the enhancement of shear modulus at room temperature due to annealing, 503 K annealed sample will have ~1.02 times of that of as-cast sample which comes from the measured difference of flexural shear modulus according the flexural stress–deflection curves (see Fig. 6a). Ω of the 503 K annealed sample at 77 K can be obtained to be ~0.7 nm^3. Then we can obtain $\frac{\Delta V^*}{V_f} \approx 10.6$ for the 503 K annealed sample from Eq. (6).

We also notice that the fracture features of the 503 K 15 min annealed sample tested at 77 K (Fig. 7b) are very similar with these of 653 K 15 min annealed sample tested at room temperature (Fig. 4f). They have similar shear offset values (~7 μm) and vein-like patterns. Then it is reasonable to think that the two samples roughly have the same Ω. Similarly, we obtain $\frac{\Delta V^*}{V_f} \approx 25.0$ for the 653 K annealed sample whose room temperature shear modulus is ~1.05 times of that of as-cast sample. From the above, we have the values of $\frac{\Delta V^*}{V_f}$ for several free volume states at the strain rate of 10^{-4} s^{-1}, where $\ln\frac{\omega_0}{C\dot{\gamma}} \approx 30$.

The variation of volume of STZ with temperature T for different sample states can be plotted in Fig. 9. For the 653 K 15 min annealed sample at 77 K, Ω was calculated to be ~0.17 nm^3 where there are only ~9 atoms involved in an STZ, which indicates the coupling of 653 K annealing and 77 K cryogenic temperature has greatly reduced Ω to be only ~5% of that of as-cast sample at room temperature (~158 atoms). It is indeed that the STZ mode has changed into TTZ mode as shown in Fig. 7f, when the volume of STZ is extremely small or close to zero as we have presumed above.

Assuming that 0.17 nm^3 is a critical STZ volume of transition from STZ mode to TTZ mode for the Vit105 alloy, it can predict a DBT temperature of ~17 K for the as-cast sample based on Eq. (6). Tabachnikova et al. [12] have shown that with the temperature decrease to 77 K from room temperature, both the compressive strength and plasticity of $Zr_{64.13}Cu_{15.75}Ni_{10.12}Al_{10}$ BMG samples could be

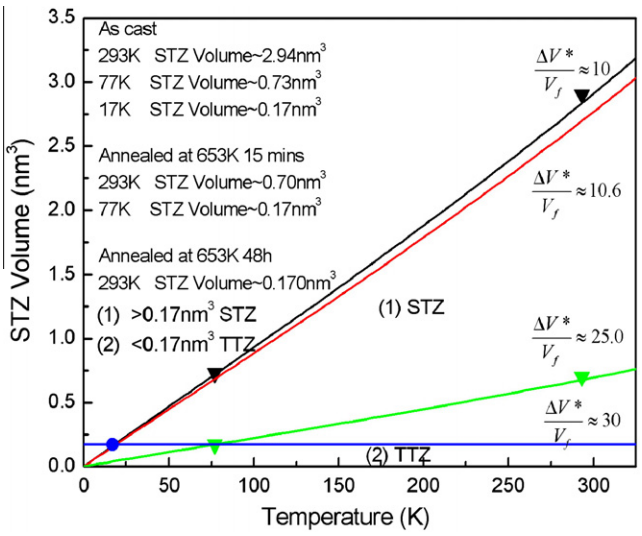

Fig. 9. Variation of volume of STZ with temperature T for different free volume states.

enhanced. When the experimental temperature was lowered to 4.2 K, the samples fractured catastrophically with poor fracture strength. This result is in good agreement with our above prediction. Moreover, the brittle failure of $Zr_{41.2}Ti_{13.8}Ni_{10}Cu_{125}Be_{225}$ at 77 K might also be ascribed to the decrease of the STZ volume due to low temperature, where nano-scaled "chevron" patterns rather than vein patterns on the low temperature fracture surface indicate an apparent decrease in the plasticity [7]. While for other BMGs [49–55] with both enhancements of yield strength and plasticity under compression when the test temperatures decrease from room temperature to liquid nitrogen temperature (77 K), a lower test temperature might introduce a brittle failure, i.e. ductile-to-brittle transition. It should be addressed that, in a certain range of cryogenic temperature, the inconsistency between the enhanced compressive plasticity and the reduced bending plasticity presented here might be associated with the actual dynamics of shear bands under different stress states. This deserves to be studied in our later work.

We further found that with the decrease of free volume, the temperature of STZ to TTZ would move to a high temperature, even room temperature with complete annealing (e.g. Group 4). The Ramamurty group [16] had systematically investigated the impact properties of some Zr-based BMGs and their results unambiguously show that the DBT temperature is a function of annealed state and increases with the severity of annealing (annealed at either high temperatures or for long durations). Here, both the annealing and test temperature can reduce the STZ volume, for the sample with more free volume, much lower temperature are needed to decrease volume of STZ, thus introduce brittle fracture whereas for the sample with less free volume, a mediated cryogenic temperature is enough to reduce the STZ volume. Then, the DBT temperature moves to a higher temperature with the decrease of free volume. This prediction is consistent with our experimental observations, that is, the 653 K 48 h annealed sample with almost no free volume shows the DBT temperature of 293 K (see Figs. 7g and h and 8c and d). In a recent paper, Uhlenhaut et al. [56] have found sharp DBT in Mg-based glasses, and the abrupt change in bending ductility is found to result from disappearing large free volume. Their results agree well with the present prediction that the STZ volume will decrease with the significant decrease of free volume to introduce the transition from STZ mode to TTZ mode.

We tried to illustrate the physical mechanism of STZ volume decrease due to annealing, cryogenic temperature and strain rate. It is well known that free volume within samples is reduced during structural annealing. The STZ operation actually is a local motion of atoms around a free volume site. Therefore, with the reduction of free volume, there will be fewer atoms to be involved in an STZ. The decrease of ambient temperature results in the enhanced activation energy of an STZ. In other words, the STZ requires the greater activation energy at lower temperatures. If the activation energy is fixed with the decreasing temperature, it can be speculated that fewer atoms can be activated in an STZ operation. The STZ operation as the unit process of plastic flow needs a certain time scale. Such time scale allows atoms to nonlinearly or irreversibly rearrange, and hence plastic flow event occurs. At higher loading rates, the atoms in samples do not have enough time to rearrange. Thus the number of the rearranged atoms is smaller, which has been confirmed by recent atomistic simulations [57]. Therefore, annealing, cryogenic temperature and higher strain rate can reduce the STZ volume via decreasing the mobility of rearranged atoms. With the decrease of STZ volume, the ability of shear band formation will decrease even to zero; in other words, STZ mode can change into TTZ mode. If two or three factors can take effect simultaneously, the transition of STZ to TTZ will be much easier.

5. Conclusion

We have performed three-point bending tests for both as-cast and as annealed Vit105 alloys at different ambient temperatures. The results indicated that the free volume decrease and/or cryogenic temperature will decrease the propensity for the formation of multiple shear bands and hence deteriorate macroscopic plasticity, and even introduce a remarkable DBT, i.e. fracture mode from ductile STZ to brittle TTZ mode. It is suggested that such DBT in BMGs corresponds to a critical value of the STZ volume. Our findings are fundamentally useful for understanding the fracture mechanism in BMGs.

Acknowledgements

The financial support from the National Natural Science Foundation of China (NSFC) under Grant Nos. 50871079, 11002144 and 50671076 is gratefully acknowledged. The authors also wish to express their special thanks for the support from the National Basic Research Program of China (Grant No. 2010CB631003) as well as 111 Project of China (B06025). This work was also supported by the Program for New Century Excellent Talents in University (China).

References

[1] Johnson WL. Mrs Bull 1999;24:42.
[2] Inoue A. Acta Mater 2000;48:279.
[3] Wang WH, Dong C, Shek CH. Mater Sci Eng R 2004;44:45.
[4] Schuh CA, Hufnagel TC, Ramamurty U. Acta Mater 2007;55:4067.
[5] Greer AL, Ma E. MRS Bull 2007;32:611.
[6] Wu TW, Spaepn F. Philos Mag B 1990;61:739.
[7] Bengus VZ, Tabachnikova ED, Miskuf J, Csach K, Ocelik V, Johnson WL, et al. J Mater Sci 2000;35:4449.
[8] Falk ML. Phys Rev B 1999;60:7062.
[9] Ramamurty U, Lee ML, Basu J, Li Y. Scr Mater 2002;47:107.
[10] Raghavan R, Murali P, Ramamurty U. Intermetallics 2006;14:1051.
[11] Castellero A, Moser B, Uhlenhaut DI, Dalla Torre FH, Loffler JF. Acta Mater 2008;56:3777.

[12] Tabachnikova ED, Podol'skii AV, Bengus VZ, Smirnov SN, Luzgin DV, Inoue A. Low Temp Phys 2008;34:675.
[13] Kumar G, Rector D, Conner RD, Schroers J. Acta Mater 2009;57:3572.
[14] Lewandowski JJ, Wang WH, Greer AL. Philos Mag Lett 2005;85:77.
[15] Lewandowski JJ, Shazly M, Shamimi Nouri A. Scr Mater 2006;54:337.
[16] Raghavan R, Murali P, Ramamurty U. Acta Mater 2009;57:3332.
[17] Jiang MQ, Ling Z, Meng JX, Dai LH. Philos Mag 2008;88:407.
[18] Johnson WL, Samwer K. Phys Rev Lett 2005;95:195501.
[19] Zhang LC, Jiang F, Zhao YL, Pan SB, HeL SunJ. J Mater Res 2010;25:283.
[20] Slipenyuk A, Eckert J. Scr Mater 2004;50:39.
[21] Debenedetti PG, Stillinger FH. Nature 2001;410:259.
[22] Spaepen F. Acta Metall 1977;25:407.
[23] Jiang F, Zhao YL, Zhang LC, Pan SB, He L, Sun J, et al. Adv Eng Mater 2009;11:374.
[24] Inoue A, Zhang T, Masumoto T. J Non-Cryst Solids 1993;156:598.
[25] Conner RD, Johnson WL, Paton NE, Nix WD. J Appl Phys 2003;94:904.
[26] Ravichandran G, Molinari A. Acta Mater 2005;53:4087.
[27] Hufnagel TC, El-Deiry P, Vinci RP. Scr Mater 2000;43:1071.
[28] Dalla Torre FH, Klaumunzer D, Maass R, Loffler JF. Acta Mater 2010;58:3472.
[29] Christiansen A, Shortall JB. J Mater Sci 1976;11:1113.
[30] Xi XK, Zhao DQ, Pan MX, Wang WH, Wu Y, Lewandowski JJ. Phys Rev Lett 2005;94:125510.
[31] Pan DG, Zhang HF, Wang AM, Wang ZG, Hu ZQ. J Alloys Compds 2007;438:145.
[32] Wang G, Zhao DQ, Bai HY, Pan MX, Xia AL, Han BS, et al. Phys Rev Lett 2007;98:235501.
[33] Nagendra1 N, Ramamurty U, Goh TT, Li Y. Acta Mater 2000;48:2603.
[34] Zhang ZF, Eckert J, Schultz L. Acta Mater 2003;51:1167.
[35] Zhang ZF, Eckert J. Phys Rev Lett 2005;94:094301.
[36] Zhang Y, Greer AL. Appl Phys Lett 2006;89:071907.
[37] Demetriou MD, Harmon JS, Tao M, Duan G, Samwer K, Johnson WL. Phys Rev Lett 2006;97:065502.
[38] Falk ML, Langer JS. Phys Rev E 1998;57:7192.
[39] Jiang MQ, Wang WH, Dai LH. Scr Mater 2009;60:1004.
[40] Chen HM, Huang JC, Song SX, Nieh TG, Jang JSC. Appl Phys Lett 2009;94:141914.
[41] Zhang HW, Maiti S, Subhash G. J Mech Phys Solids 2008;56:2171.
[42] Jiang MQ, Dai LH. J Mech Phys Solids 2009;57:1267.
[43] Pan D, Inoue A, Sakurai T, Chen MW. PNAS 2008;105:14769.
[44] Orowan E. Z Phys 1934;89:327.
[45] Dubach A, Dalla Torre FH, Loffler JF. Acta Mater 2009;57:881.
[46] Zink M, Samwer K, Johnson WL, Mayr SG. Phys Rev B 2006;73:172203.
[47] Argon AS. Acta Metall 1979;27:47.
[48] Bletry M, Guyot P, Blandin JJ, Soubeyroux JL. Acta Mater 2006;54:1257.
[49] Takeuchi S, Kakegawa T, Hashimoto T, Tsai AP, Inoue A. Mater Trans JIM 2000;41:1443.
[50] Li HQ, Fan C, Tao KX, Choo H, Liaw PK. Adv Mater 2006;18:752.
[51] Kawashima A, Okuno T, Kurishita H, Zhang W, Kimura H, Inoue A. Mater Trans 2007;48:2787.
[52] Okuno T, Kawashima A, Kurishita H, Zhang W, Kimura H, Inoue A. Mater Trans 2008;49:513.
[53] Huang YJ, Shen J, Sun JF, Zhang ZF. Mater Sci Eng A 2008;498:203.
[54] Klaumunzer D, Maass R, Dalla Torre FH, Loffler JF. Appl Phys Lett 2010;96:061901.
[55] Vinogradov A, Lazarev A, Louzguine-Luzgin DV, Yokoyama Y, Li S, Yavari AR, et al. Acta Mater 2010;58:6736.
[56] Uhlenhaut DI, Dalla Torre FH, Castellero A, Gomez CAP, Djourelov N, Krauss G, et al. Philos Mag 2009;89:233.
[57] Jiang MQ, Jiang SY, Ling Z, Dai LH. Comput Mater Sci 2009;46:767.